# Screw-Generated Forces in Granular Media: Experimental, Computational, and Analytical Comparison

**Andrew Thoesen, Sierra Ramirez and Hamid Marvi***
School for Engineering of Matter, Transport and Energy (SEMTE), Arizona State University, Tempe, AZ 85251

*DOI 10.1002/aic.16517*
*Published online in Wiley Online Library (wileyonlinelibrary.com)*

*This study presents an experimental, computational, and analytical comparison of a submerged, double-helix Archimedes screw generating propulsive force against a bed of glass beads. Three screws of different pitch lengths were studied. Each screw was tested at six speeds in approximately 10 trials for a total of 180 experimental trials. These experiments were then replicated in EDEM, a discrete element method (DEM) software program. DEM simulation results for thrust forces in the 30–120 rpm regime had a 5%–20% inflation of forces compared to experimental results. These simulations were then compared with resistive force theory (RFT) plate approximation of the screw geometries. We analyze a superposition-based partition approach to the full-length screws as well as force generation in shortened, one- and two-blade screws. We find that the force generation is dependent on the flow patterns and cannot be reduced to partitioned approximations as with simple intruders.* © 2018 American Institute of Chemical Engineers *AIChE J*, 00: 000–000, 2019
*Keywords: granular media, discrete element method, resistive force theory, screw*

## Introduction

The current state of granular media modeling encompasses many approaches. Techniques such as resistive force theory (RFT) illustrate that granular intruders can be evaluated as a collection of smaller, simple structures and added together for many different shapes.[1-5] Recently, advancements have been made using continuum modeling, which treats granular media as a continuum uniform body.[6-8] Evidence suggests that RFT and continuum approaches can be explained by plasticity theories[9] and both have also been experimentally validated.[3,10] In contrast, discrete element method (DEM) is a computational approach widely used for studying granular media. Unlike the former methods, which create analytical solutions from empirical data or treat granular media as a continuum, DEM models the granular terrain by simulating each individual particle or an approximation thereof. This provides a future path for experiments, which may be difficult to replicate or characterize responses for.[11,12]

Studies examining the comparisons between DEM simulations and granular media experiments mainly focus on either of the following two aspects: the flow patterns of the granular material[13-19] or the generated reaction forces of a variety of machines. Much of the literature focuses on the tumbling and mixing patterns of drums or other rotating items.[20-23] Others study blending and mixing[24-27] machines. Utilizing screw conveying of both powder and beaded material is another topic of interest in the literature.[28-34] This study presents experiments, DEM simulations, and RFT approach on a comparative basis to evaluate the reaction forces on a screw embedded in granular media and the best approaches to estimate them.

Comparative results between DEM simulations and experiments can vary widely. There is generally good agreement, but it is necessary to identify what granular media qualities are essential for a particular comparison. For example, there is very close experimental validation for recent developments in granular scaling laws[10] for locomotion. This also serves to show another DEM strength not easily replicated: testing gravity variation, as it effects granular compaction in locomotion. Recent cone crusher comparisons showed only slight variation in the size distribution of produced rocks between simulations and experiments.[35] However, the power draws of the rock crusher had significant errors. Likewise, pellets evaluated in DEM utilizing a variety of parameter combinations showed that several combinations produced good comparisons for a rotating drum.[36] The upper and lower angles of repose during rotation matched well with experiments, but DEM significantly overestimated particle velocities near surface level. DEM has also been used for comparisons with noncylindrical drums.[37] In another drum experiment, fluid approximation resulted in good match for speed, but pressure and particle front showed difference.[38] These can also be evaluated from a thermodynamic point of view.[39] Flow patterns for relatively small particles in hoppers have been shown to be accurately simulated.[40] Wall smoothness can often change frictional effects and introduce significant differences between experimental and DEM results in terms of flow patterns and forces.[41-43] Granular intruders have been successfully simulated when compared to experiments as well.[44] In addition, particles of similar size to ours (1–3 mm) have been simulated in many ways[45-48] as have glass beads.[49,50] These experiment-and-simulation comparisons indicate that DEM simulations have the potential to accurately recreate a wide variety

Additional Supporting Information may be found in the online version of this article.

Correspondence concerning this article should be addressed to H. Marvi at hmarvi@asu.edu

© 2018 American Institute of Chemical Engineers

of granular media scenarios. The particular scenario in this article had shown good preliminary matching between experiments and simulations[51] and was explored further.

We would like to explore whether reaction force generation in shallow submersion with a well characterized media can be approximated using DEM under two conditions: while reducing the Young's modulus to a level that allows feasible computation times, and with a complex, helical intruder such as a screw. This was done with the aim of moving simulations to a cohesive, reduced gravity environment. The ability to experimentally verify a granular media in earth gravity and to confidently extrapolate results in lower gravity would be an invaluable design tool for space applications. To achieve this goal, we performed experimental, computational, and analytical studies of screws buried just below the surface of soda-lime glass beads. The experimental results and trends for both thrust and vertical forces are discussed first, followed by simulation results, and then a direct comparison of the two. This is followed by a discussion on the nature of force generation in screws and the feasibility of using RFT for studying the screw-generated forces. Finally, discrepancies in all cases and sources of error are discussed, and we conclude with potential future paths for this work.

## Methods

### *Experiments*

Experiments were conducted in a 20 cm × 100 cm bed of glass beads with approximately 15 cm of depth. Three screws with dimensions of 10 cm axial length and 5 cm diameter were designed in Solidworks and printed using arylonitrile butadiene styrene (ABS) on a Stratasys three-dimensional (3D) printing system as shown in Figure 1. Pitch lengths of 4, 6, and 8 cm were used. These screws will be referred to as P4, P6, and P8, respectively. As shown in Figure 1, the ABS plastic screw was connected to a metal shaft collar coupling. This was then connected to a 12 V Pololu motor. The motor was housed inside a motor casing created with the same printer as the screw. The back cover of the motor casing was then attached to a six degree-of-freedom load sensor (interface force measurement solutions, 6A27A-F11) using a laser-cut acrylic attachment with six screws. The other side of the sensor was secured to another laser-cut acrylic piece attached to a vertical aluminum rod and locked into place.

Horizontal leveling of the motor box was measured using an electronic angle measurement device to ensure horizontal alignment. Next, the load cell was zeroed when steady. This is after running the load cell for a minimum of 45 min to minimize the drift. About 8 mN/min load cell drift is seen in a typical trial. Then recording began before the test area was filled with beads. The 2-mm glass beads were added such that the screw was completely immersed. The surface level of beads was smoothed for each trial and churned beforehand to avoid compaction or influences of previous trials. Six speeds were used: 30, 45, 60, 75, 90, and 105 rpm. Each trial ran for approximately 15–20 s to ensure steady-state values. After 10 trials, the setup was unloaded by removal of all bead contacts with the motorbox, screw, and other items. Measurements were then taken for 10 s. Any differences between the unloaded values before and after the experiment were noted. Due to the thermal drift, the average of the zeroing before and after experiments was subtracted from the average of all trials. The motor control and rpm data collection were driven by an Arduino Uno.

### *Simulations*

Using the model developed in Solidworks, we set up simulations in EDEM, a DEM program (Figure 2). The imported model was then placed inside a simulated cylindrical bed. The simulated environment was filled with particles composed of two overlapping spheres, which were slightly offset from each other. This was done to introduce an aspect ratio of 1.1 to eliminate perfect sphericity to correlate with the manufacturer's given 90% roundness. This has been shown[52] to have a significant effect in DEM simulations. The degree of eccentricity does not seem to be as influential as its presence. For example, the difference in flow patterns between a perfect sphere and a 1.1 aspect ratio particle is much larger than between a 1.1 and 1.2 aspect ratio particles. The particles were also polydispersed in a normal distribution with standard deviation of 0.1 mm per the manufacturer's specifications. We allowed particles to settle until we observed no movement. Both simulations and experiments

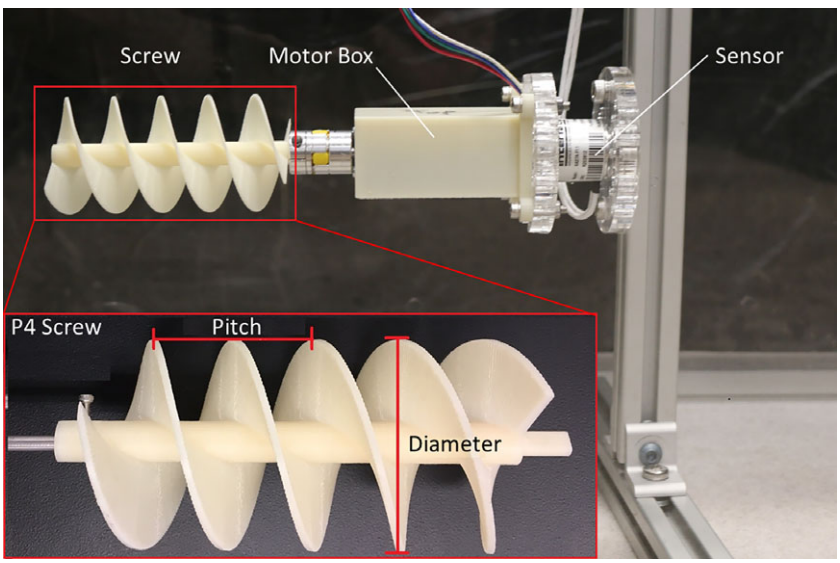


**Figure 1. Experimental setup.**
**[Color figure can be viewed at wileyonlinelibrary.com]**

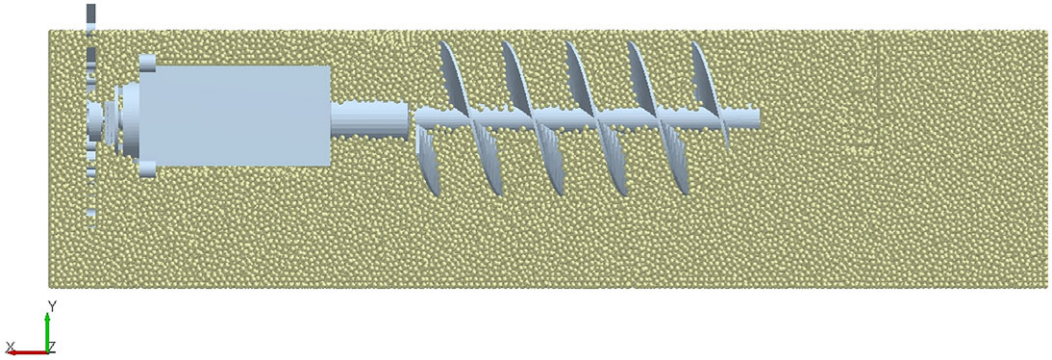

**Figure 2. EDEM model with P4 screw (side view).**
**[Color figure can be viewed at wileyonlinelibrary.com]**

began with the screw completely covered by granular media. The amount of screw covered was not different across trials in either experiment or simulation, or to each other. The horizontal screw was tangential to the surface of beads. Its blades touched the last layer of beads. At this point, we began the kinematic motion of the screw at the specified rotational velocity instantaneously. We ran it until steady state was observed for 2 s; this required at least 7 s of simulation. Steady state was defined as a deviation of <1% with the previous 1-s average. The details of the DEM contact model are explained in the Potential sources of error section.

EDEM allows user control over almost all aspects of the simulated granular material and geometry materials. In addition to shape, there are six mechanical properties we will highlight that influence the simulated flow patterns. Three of these are material properties: density, Young's modulus, and Poisson's ratio. These parameters are well-established for soda-lime glass.[53] The manufacturing method of ABS affects the mechanical

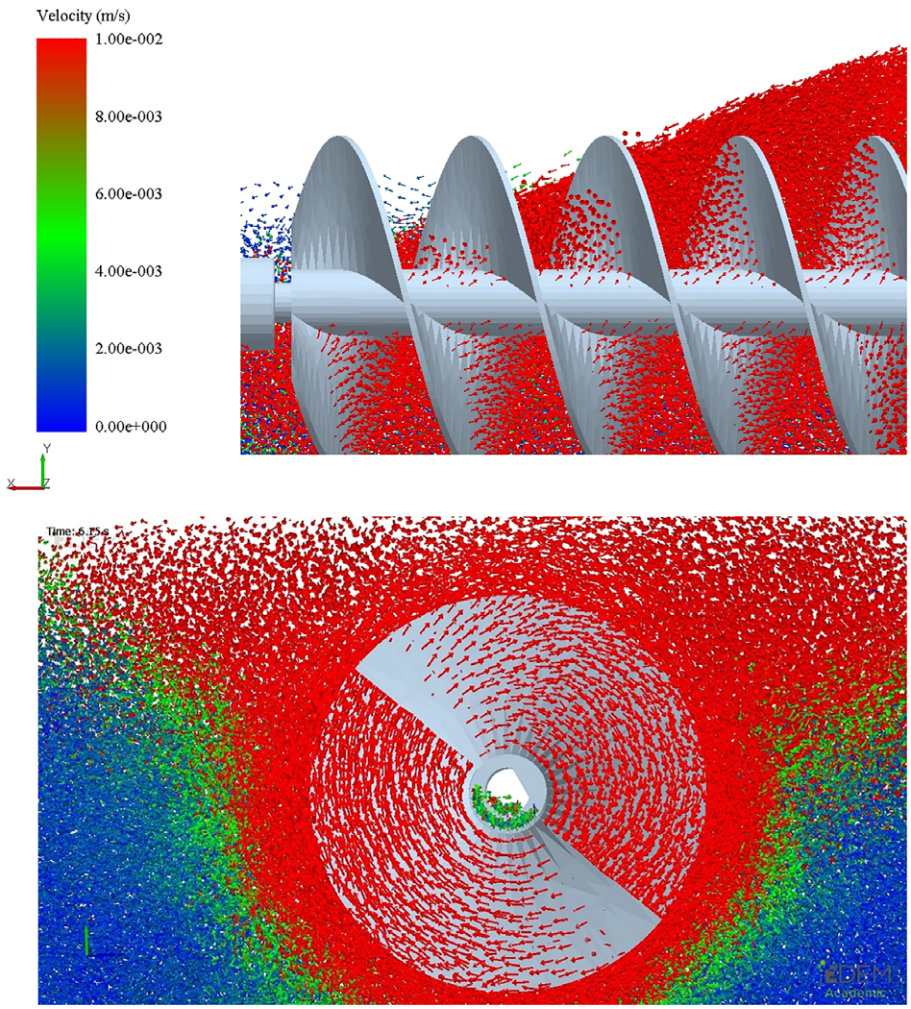


**Figure 3. Flow visualization of particles in side and front views.**
**[Color figure can be viewed at wileyonlinelibrary.com]**

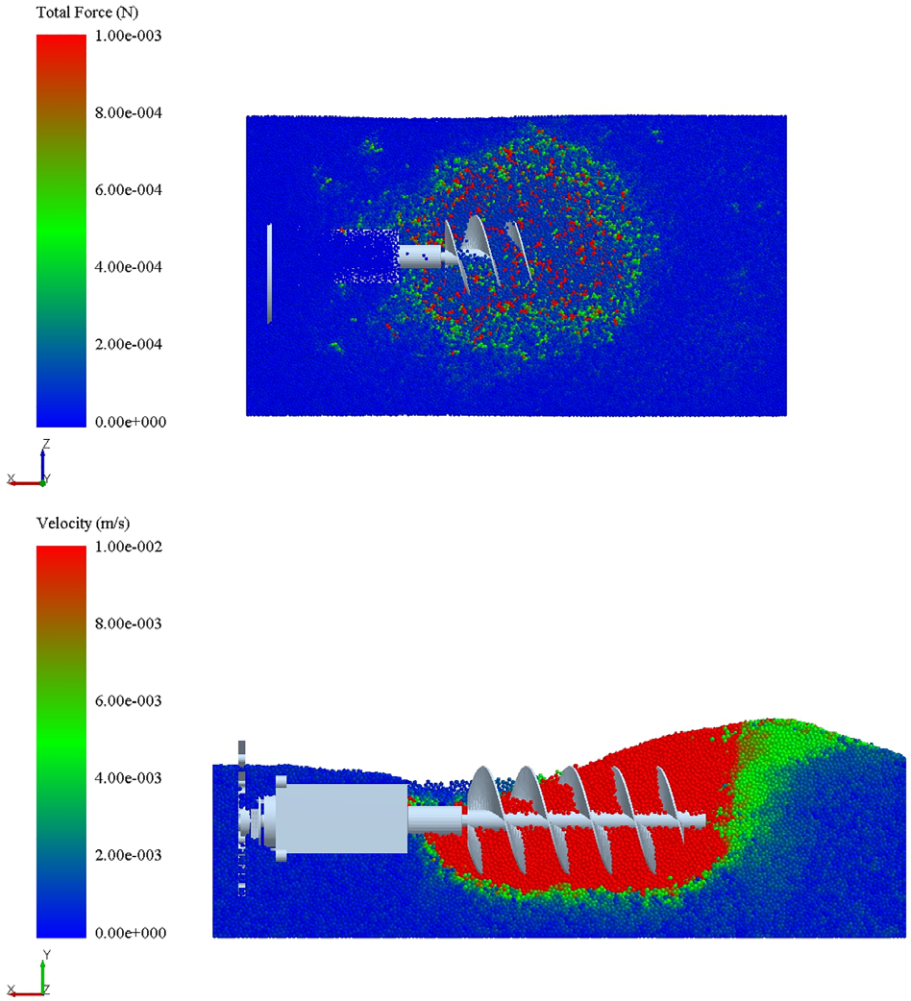


**Figure 4. Buildup of particles from top and side views and colored by force and velocity respectively.**
**[Color figure can be viewed at wileyonlinelibrary.com]**

properties of the plastic, but recent tests have established baselines for 3D-printed ABS parts.[54] There are three remaining properties that are interaction-dependent: coefficient of restitution, static friction, and rolling friction. These are different between glass–glass interactions and glass–ABS interactions. Several experiments have looked at glass–glass interactions with beads of comparable size to ours. The coefficient of restitution with isolated bead collisions taken from high-speed camera tests in the literature[55,56] estimate the value at 0.97 for collision speeds under 1 m/s. The same studies estimate the dynamic coefficient of friction at 0.092 and the static coefficient of friction at between 0.16 and 0.29. We performed a sample glass–glass static friction test and found values similar to the lower end at 0.16. The rolling friction coefficient of glass beads against each other is estimated at 2.5e-5 to 5e-5.[57]

We did not find glass–ABS interaction properties reported in the literature. The coefficient of restitution for several different 3D-printed materials has been measured before.[58] Researchers used an aluminum rod at various speeds on plastic plates composed of these materials.[58] The coefficient of restitution will also change based on the order of magnitude of velocity. The impact speeds for this study are comparably lower (below 0.5 m/s) than in our study, and hence the value of 0.7 was selected as the best approximation. Because the glass–ABS interaction properties were not reported in the literature, we conducted our own measurements. For static friction, an inclined plane test was conducted. Static friction of glass–ABS was estimated at 0.16, similar to that of glass–glass. In addition, a standardized ASTM rolling friction test was adapted[59] resulting in a rolling friction of 0.173 for glass–ABS interaction.

The simulated bed is 32 cm long and 20 cm in diameter. We looked at force/velocity imaging for simulated particles, an example of which is shown in Figure 4. We could not observe any wall effects present, and particle forces were below 0.0002 N at walls as shown. The piles formed at the end of the bed had the same shape/height/extent in experiments and DEM. This was an item of concern we considered before beginning simulations and took care to avoid.

## Results and Discussion

### *Experiments*

The experimental force data were taken from the steady-state plateau of each individual trial for multiple seconds and averaged, per trial. All trials were then averaged with standard error shown in the plots. A force graph of what an experimental trial run looks like is shown in Figure 5a and that of simulation is shown in Figure 5b. The simulation takes slightly longer to reach steady state, but the force evolves in a similar manner. As each combination of design and speed was only simulated once, there is no standard deviation to speak of for DEM simulations. The given values are the mean force over

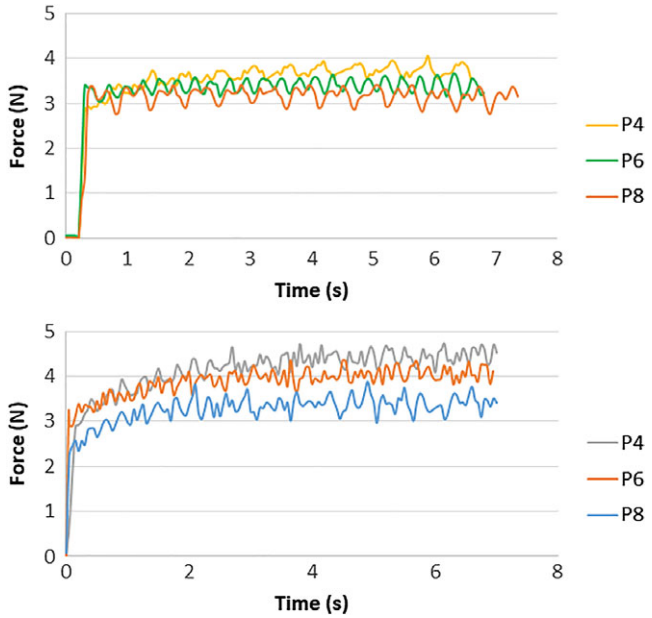


**Figure 5. Thrust force vs. time at 105 rpm for (a) experiments vs. (b) simulations.**
**[Color figure can be viewed at wileyonlinelibrary.com]**

the last 2 s of data, and the noise oscillations are typically within a 0.5 N band.

All experimental results for thrust force as a function of rpm are shown in Figure 6a. As the pitch is shortened and an increased amount of surface area faces the axial direction, thrust force increases. The force also increases with rpm, but inertial forces are not the primary contributor to the magnitude of thrust force in this case. For experiments, the thrust force increases from lowest to highest rpm for P4, P6, and P8 were 11.9%, 4%, and 13.6%, respectively. These results are within the range of other observations for increased force in granular media due to inertial forces. For example, <20% increase in forces on intruders was observed when velocity was increased from 1 cm/s to 1 m/s.[3]

In contrast to the horizontal thrust force data in Figure 6a, the vertical force data in Figure 7a show virtually no relationship between vertical force and rpm, nor vertical force and screw pitch. The vertical force changes from 30 rpm to 105 rpm in experiments were − 1%, −10%, and 5% for P4, P6, and P8, respectively. Figure 7b shows a different story for simulations as P4, P6, and P8 vertical forces increase by 10.3%, 8.5%, and 8.6% from lowest to highest speed, respectively. In these experiments, as previously mentioned, the trial begins with the leveled surface tangential to the screw blade as shown in Figure 2. It ends with a steady state mound at the expelling end, as shown in Figure 4, continually regenerated from beads falling after the angle of repose is exceeded. Note that these results, indicating small vertical force compared to the axial force, are limited to surface conditions. We cannot extrapolate them to the force relationship a deeply buried screw may experience.

### *DEM simulations*

Thrust data for simulations are shown in Figure 6b. A plateau appears at the end of the curve. Because of the screw's surface level, the majority of force being generated comes from the accumulated pile of material near the discharging side. While the rpm cannot change the angle of repose, a faster speed can continue to recirculate and deposit material at a higher rate, resulting in more thrust force. Hence, at higher speeds, we see a mild increase in force. It appears that thrust forces begin to plateau at high speeds. The avalanching slope of the mound does not reach the boundary of simulation or experiment according to our observations. Figure 4 shows that boundary particles are not significantly affected. During both experiment and simulation, we were cognizant to examine the incoming data and observe that no wall effects were present.

The plateau can be explained if we think of the affected area around the screw as a control volume. As the screw speeds up,

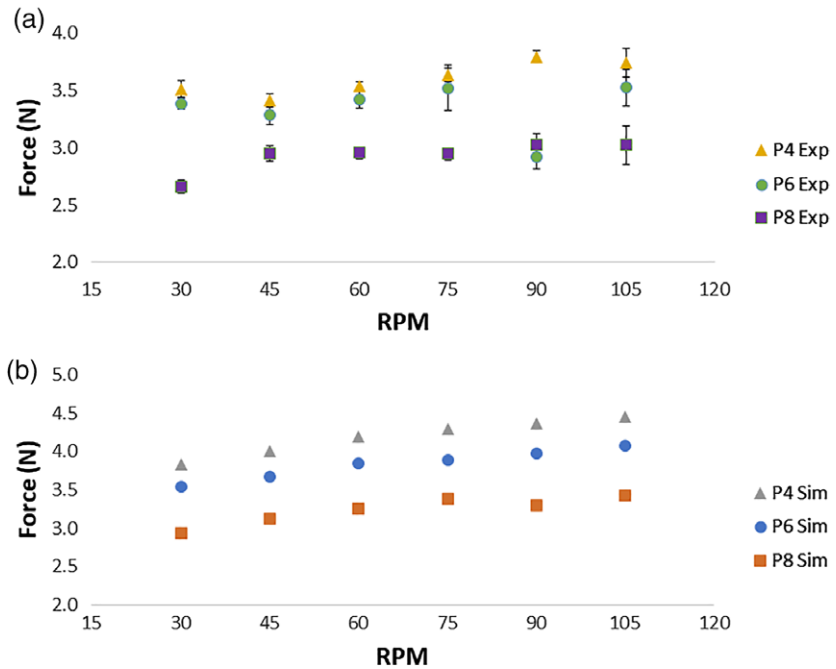


**Figure 6. Thrust force. (a) Experiments vs. and (b) simulations.**
**[Color figure can be viewed at wileyonlinelibrary.com]**

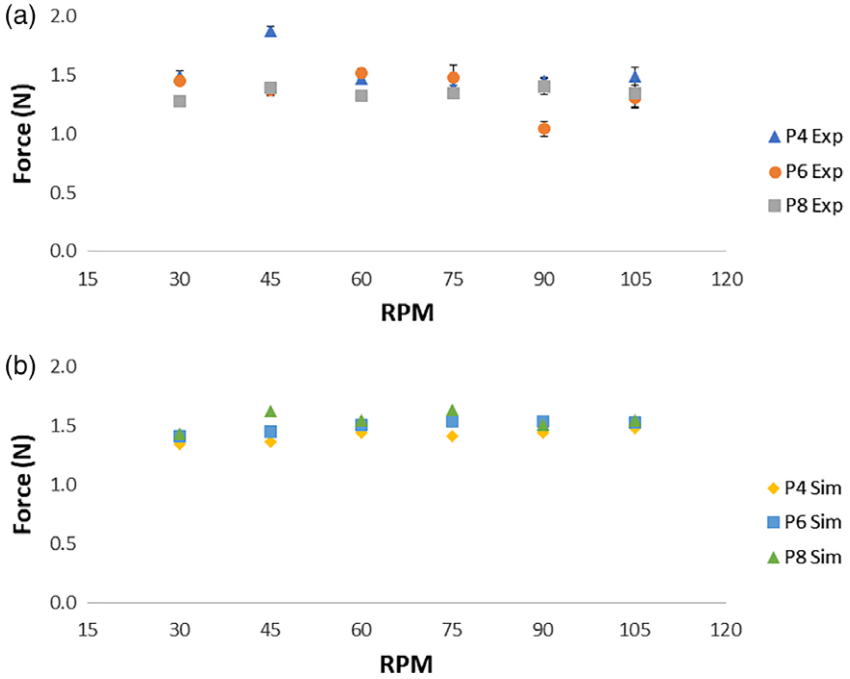


**Figure 7. Vertical force. (a) Experiments vs. and (b) simulations.**
**[Color figure can be viewed at wileyonlinelibrary.com]**

the mass flow rate of particles out of this control volume begins to increase. However, the maximum mass flow rate of particles into the control volume, or "refill rate," is a function of both gravity (the acceleration forces pushing the particles downward to open space) and particle's angle of repose and thus, it does not change. At a high enough speed, the mass flow rate of particles out of the control volume begins to equal or exceed the maximum mass flow rate into the control volume. This is analogous to a choked flow in fluid dynamics.

As shown in Figure 6b, the band between higher and lower speeds stays consistent. For P4, P6, and P8, the amount of force increase from 30 rpm to 105 rpm is 15.5%, 15.3%, and 16.7%, respectively. Similar to experiments, the simulation forces in Figure 7b do not show much magnitude difference in the vertical direction. In particular, P4, P6, and P8 vertical force increases are 10.3%, 8.5%, and 8.6% from highest to lowest speed, respectively.

As shown in Figure 6, the average thrust force increase from experiment to simulation across all rpms is 16.0%, 15.2%, and 10.6% for P4, P6, and P8. The average vertical force difference between experiment and simulation across all rpms is −5.4%, 12.1%, and 15.2% for P4, P6, and P8, respectively. Some of the sources contributing to these differences in magnitude will be discussed in the error section.

### *Resistive force theory*

One recent approach to assess granular mobility and force generation is RFT. Under the assumptions of negligible inertial forces and using superposition of geometric components, RFT examines the forces on geometries in granular media. It does so by characterizing the shape into discrete plate elements. These plate elements, based on orientation, are compared with previously acquired data in various granular media. As long as these elements are independent and do not influence each other, they can be added together.[60] The forces are derived from empirical equations found through evaluation of a flat plate at different orientations and velocities. By applying a Fourier transform to the data of multiple granular media, empirical equations were obtained that linked the forces generated as a function of orientation angle and velocity vector.

We applied an RFT approach to our horizontal, helical screw under the assumption that it could be well approximated with small plates. Estimations of our total screw force correlated poorly between experiments and RFT (see Supporting Information A). The RFT estimated forces were 10.34 N for a 2-cm (half-pitch) P4 screw buried at 4 cm and 19.90 for a 10-cm P4 screw with upper blades located just at surface level of the granular media, compared to 4.51 N for P4 DEM simulations. This prompted a closer investigation into the mechanics of how a screw generates force in granular media. We conducted a DEM simulation where the depth of the screw was increased to 4 cm instead of just below the surface level. This ensured that the depth would stay consistent rather than the material piling to one side as with the surface case.

As shown in Figure 8, the last 2 cm (a half pitch-length or "turn") of the 10-cm-length screw generated 55.8% of the total force. The last 4 cm, a full turn, generated 63.1% of the total force. RFT would predict uniform force generation across the screw if none of the geometry was interfering with other sections. Therefore, the initial conclusion for RFT failing to reproduce the forces was that the current designs were violating superposition by introducing leading edges. A leading edge is a portion of the object's geometry that is in front of another portion of the object in the direction of travel. By doing this, the first portion affects the flow pattern applied to the second portion. This violates a key aspect of superposition, namely that the additive portions do not affect each other. Each chamber was moving the material forward along a path that the proceeding chamber had already cleared. The section of the screw pushing granules against a bulk of granules and generating the majority of the force is the expelling end.

The above insights prompted an investigation to see whether perhaps a screw that did not violate the leading edge assumption would correlate better to a plate approximation.

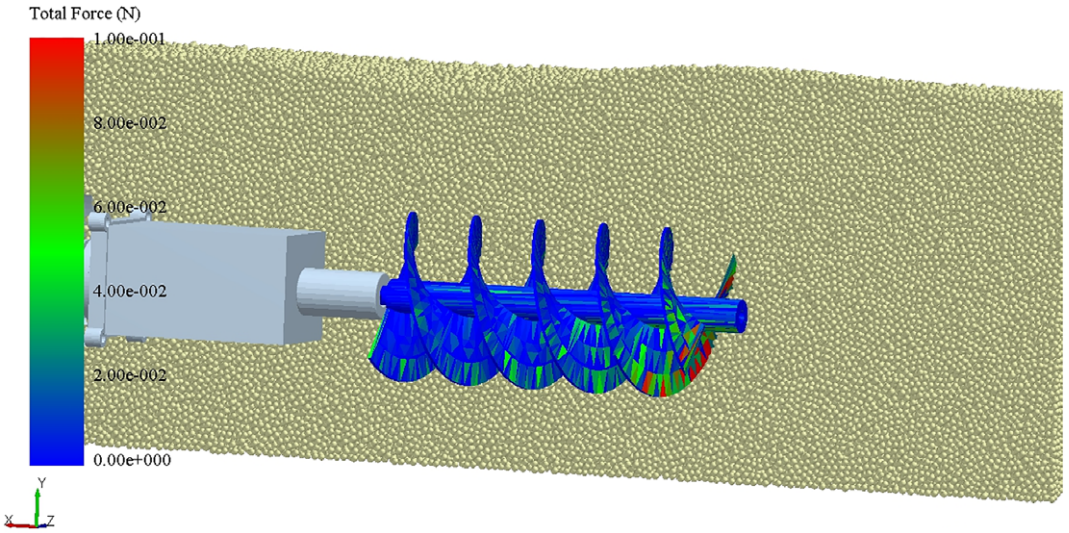


**Figure 8. These instantaneous forces occurring at the given time across the discretized screw in the simulation are unevenly distributed, showing much stronger forces generated at the expelling end (right side of the screw).**

**[Color figure can be viewed at wileyonlinelibrary.com]**

We ran similar simulations but with screws of half-pitch length instead of the full 10 cm so that the leading geometry assumption would not be violated.

We used a 2-cm P4 screw as the sample. The screw was placed at 4 cm depth and run at 15 and 30 rpm with negligible difference. This is within the range of depth tested during the experiments used to create the empirical RFT approximation equations. The results of this indicated a force generation of approximately half of that predicted by RFT estimations.

This prompted another investigation into whether force generation per screw blade would be additive. We refer to the number of blades in the screw designation by "N" followed by a number. An N1 screw, a screw with only one helix winding, was evaluated in the same depth as the N2 screw. For the buried P4 N2, we obtained 5.5 N axial force. For the buried P4 N1 in identical conditions, we obtained an oscillating force of 2–5 N depending on blade orientation. To construct the hypothetical force of a screw with two of these blades, we took the results, offset by a half-cycle, and summed those forces. The N1, N2, and theoretically constructed N1 + N1 are shown in Figure 9. The results indicate that added blades do not scale linearly even under ideal conditions. This perhaps seems intuitive in hindsight, especially compared to bladed geometries interacting with fluids, but it was unclear whether slow movement in granular media would hold to the same rule. This indicates that RFT which relies on superposition should be approached with caution when applying to screw-generated forces in granular media.

Indeed, the flow pattern of the screw is of utmost importance to the force generation if we compare results from a full 10-cm screw and a half-pitch screw. The last 2 cm of the 10-cm P4 screw generated 4.5 N of force. In comparison, the 2-cm screw with an identical section by itself generates 5.5 N of force. This shows the importance of the previous screw sections in affecting the flow pattern and hence the amount of force a screw will generate.

### *Potential sources of error*

As discussed earlier, DEM uses a different approach from analytical methods such as continuum mechanics or empirical methods such as resistive force theory.[9,61] Each individual particle is modeled as to affect the other particles. There are different physics models that can be selected for DEM simulations based on the attributes of the granular media. Some models incorporate cohesion, adhesion, machine wear, and other aspects. The Hertz–Mindlin model was selected based on the need for a robust model without requiring wear, thermodynamics, or other analysis. The model is built on Hertzian contact theory while integrating tangential forces, damping forces, and friction forces. In this model, normal contact forces, $F_n$, are functions of the specific Young's modulus, $E^*$, the specific radius of particles, $R^*$,

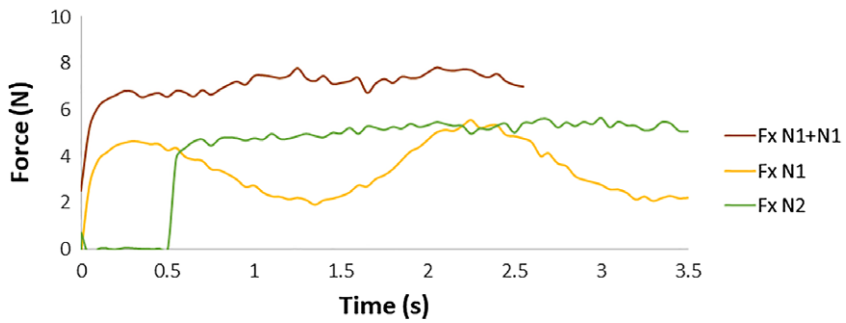


**Figure 9. The force of a double-bladed screw is significantly smaller than the sum of two single bladed screws.**

**[Color figure can be viewed at wileyonlinelibrary.com]**

and the overlap, $\delta_n$. The $i$ and $j$ subscripts denote two subsets of qualities for the two particles colliding. As the physics model is driven by a spherical contact, it looks at many calculations for the two individual spheres, where each one has its Young's modulus, radii, and so on. The $E^*$ and $R^*$ are then called the "specific" quality of the calculation. The specific Young's modulus is a function of the Young's modulus and the Poisson's ratio, $\nu_i$, of the two particles colliding. During particle collision, the simulation creates a small overlap representing an estimated real world deformation. The higher the Young's modulus, the smaller the allowable deformation. The smallest allowable deformation determines the time step of the simulation due to more frequent checks. A higher Young's modulus would allow less deformation, which requires the program to check the simulations with a much higher frequency.

$$F_n = \frac{3}{4} E^* \sqrt{R^*} \delta_n^{\frac{3}{2}} \tag{1}$$

$$\frac{1}{R^*} = \frac{1}{R_i} + \frac{1}{R_j} \tag{2}$$

$$\frac{1}{E^*} = \frac{1-\nu_i^2}{E_i} + \frac{1-\nu_j^2}{E_j}. \tag{3}$$

A DEM time step is therefore a function of particle stiffness. Real modulus values make EDEM simulations computationally costly. This leads to a decision to reduce Young's modulus by several orders of magnitude.[57,62-65] For clarity, a reduction of magnitude by 100 results in 10 times faster simulation times in this case.[66]

Bulk behavior such as the angle of repose does not change significantly until Young's modulus has been lowered beyond the 10 MPa range.[66] Materials close to this range of stiffness (or lack thereof) will begin to see their piles collapse under their own weight for most materials. However, flow behavior may change if significant overlap is allowed with geometry. Thus, we modify Young's modulus to examine the difference in simulation results with our chosen value for stiffness (20 MPa) vs. a value closer to the measured stiffness of glass (680 MPa, 1% of the real world value). We saw a modest decrease in overall thrust force of 4.31 N to 3.9 N when adjusting particle stiffness from 20 to 680 MPa. This is due to the decrease in overlap between flowing particles and thus packing less particles into the same volume that the screw is pushing against.

The reduced particle stiffness introduces some uncertainty into the simulations. The key aspect for our study is that the particles are pressed against themselves as well as against a complex geometry. When Young's modulus reduction was analyzed,[66] the possibility of force changes was discussed. The takeaway is that Young's modulus reduction can cause different forces for simulations than their real-world counterparts when particle compression against geometries or particles is a significant feature of the flow. However, this difference was shown to be predictable and consistent in our particular case. In addition, experimental errors may also contribute to the modest discrepancies between experiments and simulations. In particular, load cell drift, minor screw misalignment, variabilities in mechanical properties, and 3D-printed imperfections may play a part in slight differences observed between experimental results and DEM simulations.

## Conclusion

The primary driving goal of this research was the evaluation of DEM capabilities for accurately predicting the forces generated by double-wound helices using a well-characterized granular material. DEM is valuable for complex geometries which may violate leading edge geometry conditions assumed in RFT or continuum modeling to find accurate solutions. In particular, by using a well-characterized material, we show that it is possible to make reasonably accurate predictions about helix force generation with DEM at lower Young's modulus values within the explored range of speed, size, and granular material. In contrast, we observed that a rotating helix in granular media may not be well analyzed using RFT.

We evaluated three screw designs at six rotational speeds with approximately 10 trials for each speed experimentally. We evaluated those same screw designs with DEM software using adjustments to Young's modulus as suggested allowable in the literature.[66] The difference between experimental and simulation results for thrust force in overall magnitude was within 5%–20% for all screws. Addressing the differences in simulations and experiments leads to the conclusion that DEM is suited for evaluating forces generated by double-wound helices in well-characterized granular media.

## Future Work

The future work based on this study is primarily defined on two paths. The first is exploration of dynamic screws using both DEM and experimental approaches. This relies on creating multibody dynamics (MBD) simulations coupled with DEM, which can simulate rover motion in granular media. By performing these cosimulations, we can also find out what influence, if any, Young's modulus reduction has on dynamic movement characteristics such as drag force and peak velocity. The second path is experimental and simulation comparisons involving a more complex and relevant granular material. We would like to characterize lunar simulants for DEM simulations. While these particles typically exist in size on the order of 100 μm, there have been studies that show that scaling small particles up to an acceptable size for simulation still results in accurate predictions of forces on agricultural tools at a macroscopic level.[67] If this material can be characterized successfully in Earth gravity, then it may be possible to predict forces on crafts and tools in reduced gravity. Experimental studies that test reduced gravity solutions on Earth may not take the difference of gravitational compaction into account,[68] and therefore this would be a new advancement in designing for space environments. Successful characterization would be valuable to the space community and aid in vehicle design for both lunar and asteroid mobility.

## Acknowledgment

The authors would like to thank Professor Heather Emady and Spandana Vajrala for fruitful discussions on DEM simulations, Vidu Jayanetti for help with the supporting videos, and Arizona State University for funding.

## Literature Cited

1. Maladen RD, Ding Y, Umbanhowar PB, Kamor A, Goldman DI. Mechanical models of sandfish locomotion reveal principles of high performance subsurface sand-swimming. *J Roy Soc Interface*. 2011; 8(62):1332-1345.
2. Ding Y, Sharpe SS, Masse A, Goldman DI. Mechanics of undulatory swimming in a frictional fluid. *PLoS Comput Biol*. 2012;8(12): e1002810.
3. Li C, Zhang T, Goldman DI. A terradynamics of legged locomotion on granular media. *Science*. 2013;339(6126):1408-1412.

4. Zhang T, Goldman DI. The effectiveness of resistive force theory in granular locomotion. *Phys Fluids*. 2014;26(10):101308.
5. Aydin YO, Chong B, Gong C, et al. Geometric mechanics applied to tetrapod locomotion on granular media. *Conference on Biomimetic and Biohybrid Systems*. Springer; 2017:595-603.
6. Kamrin K. Nonlinear elasto-plastic model for dense granular flow. *Int J Plast*. 2010;26(2):167-188.
7. Dunatunga S, Kamrin K. Continuum modelling and simulation of granular flows through their many phases. *J Fluid Mech*. 2015;779:483-513.
8. Dunatunga S, Kamrin K. Continuum modeling of projectile impact and penetration in dry granular media. *J Mech Phys Solids*. 2017;100:45-60.
9. Askari H, Kamrin K. Intrusion rheology in grains and other flowable materials. *Nat Mater*. 2016;15(12):1274-1279.
10. Slonaker J, Motley DC, Zhang Q, et al. General scaling relations for locomotion in granular media. *Phys Rev E*. 2017;95(5):052901.
11. Marvi H, Gong C, Gravish N, et al. Sidewinding with minimal slip: Snake and robot ascent of sandy slopes. *Science*. 2014;346(6206):224-229.
12. Bagheri H, Taduru V, Panchal S, White S, Animal MH. Robotic locomotion on wet granular media. *Conference on Biomimetic and Biohybrid Systems*. Springer; 2017:13-24.
13. Zhao Y, Yang S, Zhang L, Chew JW. DEM study on the discharge characteristics of lognormal particle size distributions from a conical hopper. *AIChE J*. 2018;64(4):1174-1190.
14. Zhao Y, Xiao H, Umbanhowar PB, Lueptow RM. Simulation and modeling of segregating rods in quasi-2D bounded heap flow. *AIChE J*. 2018;64(5):1550-1563.
15. Liu S, McCarthy JJ. Validating granular segregation rate models. *AIChE J*. 2017;63(9):3756-3763.
16. Katsuragi H, Reddy KA, Endo K. Shape dependence of resistance force exerted on an obstacle placed in a gravity-driven granular silo flow. *AIChE J*. 2018;64:3849-3856.
17. Faqih A, Chaudhuri B, Muzzio FJ, Tomassone MS, Alexander A, Hammond S. Flow-induced dilation of cohesive granular materials. *AIChE J*. 2006;52(12):4124-4132.
18. Li Y, Xu Y, Jiang S. DEM simulations and experiments of pebble flow with monosized spheres. *Powder Technol*. 2009;193(3):312-318.
19. Li Y, Xu Y, Thornton C. A comparison of discrete element simulations and experiments for 'sandpiles' composed of spherical particles. *Powder Technol*. 2005;160(3):219-228.
20. Florian-Algarin M, Méndez R. Blend uniformity and powder phenomena inside the continuous tumble mixer using DEM simulations. *AIChE J*. 2015;61(3):792-801.
21. Shirsath SS, Padding JT, Kuipers J, Clercx HJ. Simulation study of the effect of wall roughness on the dynamics of granular flows in rotating semicylindrical chutes. *AIChE J*. 2015;61(7):2117-2135.
22. Vargas WL, Hajra SK, Shi D, McCarthy J. Suppressing the segregation of granular mixtures in rotating tumblers. *AIChE J*. 2008;54(12):3124-3132.
23. Yang S, Cahyadi A, Wang J, Chew JW. DEM study of granular flow characteristics in the active and passive regions of a three-dimensional rotating drum. *AIChE J*. 2016;62(11):3874-3888.
24. Remy B, Canty TM, Khinast JG, Glasser BJ. Experiments and simulations of cohesionless particles with varying roughness in a bladed mixer. *Chem Eng Sci*. 2010;65(16):4557-4571.
25. Sudah O, Arratia P, Alexander A, Muzzio F. Simulation and experiments of mixing and segregation in a tote blender. *AIChE J*. 2005;51(3):836-844.
26. Dubey A, Vanarase AU, Muzzio FJ. Impact of process parameters on critical performance attributes of a continuous blender–a DEM-based study. *AIChE J*. 2012;58(12):3676-3684.
27. Remy B, Khinast JG, Glasser BJ. Discrete element simulation of free flowing grains in a four-bladed mixer. *AIChE J*. 2009;55(8):2035-2048.
28. Orefice L, Khinast J. DEM study of granular transport in partially filled horizontal screw conveyors. *Powder Technol*. 2017;305:347-356.
29. Fernandez JW, Cleary PW, McBride W, et al. Effect of screw design on hopper draw down by a horizontal screw feeder. In: Seventh International Conference on CFD in the Minerals and Process Indistries; 2009.
30. Owen PJ, Cleary PW. Screw conveyor performance: comparison of discrete element modelling with laboratory experiments. *Prog Comput Fluid Dyn*. 2010;10(5–6):327-333.
31. Owen P, Cleary P. Prediction of screw conveyor performance using the discrete element method (DEM). *Powder Technol*. 2009;193(3):274-288.
32. Rozbroj J, Zegzulka J, Nečas J. Use of DEM in the determination of friction parameters on a physical comparative model of a vertical screw conveyor. *Chem Biochem Eng Q*. 2015;29(1):25-34.
33. Hou Q, Dong K, Yu A. DEM study of the flow of cohesive particles in a screw feeder. *Powder Technol*. 2014;256:529-539.
34. Kretz D, Callau-Monje S, Hitschler M, Hien A, Raedle M, Hesser J. Discrete element method (DEM) simulation and validation of a screw feeder system. *Powder Technol*. 2016;287:131-138.
35. Quist J, Evertsson CM. Cone crusher modelling and simulation using DEM. *Miner Eng*. 2016;85:92-105.
36. Marigo M, Stitt EH. Discrete element method (DEM) for industrial applications: comments on calibration and validation for the modelling of cylindrical pellets. *KONA Powder Part J*. 2015;32:236-252.
37. González S, Windows-Yule C, Luding S, Parker D, Thornton AR. Forced axial segregation in axially inhomogeneous rotating systems. *Phys Rev E*. 2015;92(2):022202.
38. Leonardi A, Cabrera M, Wittel FK, et al. Granular-front formation in free-surface flow of concentrated suspensions. *Phys Rev E*. 2015;92(5):052204.
39. Yohannes B, Emady H, Anderson K, et al. Scaling of heat transfer and temperature distribution in granular flows in rotating drums. *Phys Rev E*. 2016;94(4):042902.
40. Kamath S, Kunte A, Doshi P, Orpe AV. Flow of granular matter in a silo with multiple exit orifices: jamming to mixing. *Phys Rev E*. 2014;90(6):062206.
41. D'ortona U, Thomas N, Zaman Z, Lueptow RM. Influence of rough and smooth walls on macroscale flows in tumblers. *Phys Rev E*. 2015;92(6):062202.
42. D'Ortona U, Thomas N, Lueptow RM. Influence of rough and smooth walls on macroscale granular segregation patterns. *Phys Rev E*. 2016;93(2):022906.
43. Mandal S, Khakhar D. Sidewall-friction-driven ordering transition in granular channel flows: implications for granular rheology. *Phys Rev E*. 2017;96(5):050901.
44. Pazouki A, Kwarta M, Williams K, et al. Compliant contact versus rigid contact: a comparison in the context of granular dynamics. *Phys Rev E*. 2017;96(4):042905.
45. Windows-Yule C, Parker D. Center of mass scaling in three-dimensional binary granular systems. *Phys Rev E*. 2014;89(6):062206.
46. Windows-Yule C, Douglas G, Parker D. Competition between geometrically induced and density-driven segregation mechanisms in vibrofluidized granular systems. *Phys Rev E*. 2015;91(3):032205.
47. Guillard F, Forterre Y, Pouliquen O. Origin of a depth-independent drag force induced by stirring in granular media. *Phys Rev E*. 2015;91(2):022201.
48. Thomas N, D'ortona U. Evidence of reverse and intermediate size segregation in dry granular flows down a rough incline. *Phys Rev E*. 2018;97(2):022903.
49. Parez S, Aharonov E, Toussaint R. Unsteady granular flows down an inclined plane. *Phys Rev E*. 2016;93(4):042902.
50. Lemrich L, Carmeliet J, Johnson PA, Guyer R, Jia X. Dynamic induced softening in frictional granular materials investigated by discrete-element-method simulation. *Phys Rev E*. 2017;96(6):062901.
51. Thoesen A, Ramirez S, Marvi H. Screw-powered propulsion in granular media: an experimental and computational study. In: 2018 I.E. International Conference on Robotics and Automation (ICRA) IEEE; May 21-25, 2018; Brisbane, Australia; pp. 1–6.
52. Bharadwaj R, Ketterhagen WR, Hancock BC. Discrete element simulation study of a freeman powder rheometer. *Chem Eng Sci*. 2010;65(21):5747-5756.
53. Company CR. *Handbook of Tables for Applied Engineering Science*. Chemical Rubber Company; 1970.
54. Tymrak B, Kreiger M, Pearce JM. Mechanical properties of components fabricated with open-source 3-D printers under realistic environmental conditions. *Mater Des*. 2014;58:242-246.
55. Güttler C, Heißelmann D, Blum J, Krijt S. Normal collisions of spheres: a literature survey on available experiments. 2012 arXiv preprint arXiv:12040001.
56. Foerster SF, Louge MY, Chang H, Allia K. Measurements of the collision properties of small spheres. *Phys Fluids*. 1994;6(3):1108-1115.
57. Zhou Y, Wright B, Yang R, Xu BH, Yu AB. Rolling friction in the dynamic simulation of sandpile formation. *Physica A*. 1999;269(2–4):536-553.
58. Kardel K, Ghaednia H, Carrano AL, Marghitu DB. Experimental and theoretical modeling of behavior of 3d-printed polymers under collision with a rigid rod. *Addit Manuf*. 2017;14:87-94.
59. G194-08 A standard test method for measuring rolling friction characteristics of a spherical shape on a flat horizontal plane. ASTM; 2013.

60. Maladen RD, Ding Y, Li C, Goldman DI. Undulatory swimming in sand: subsurface locomotion of the sandfish lizard. *Science*. 2009;325(5938):314-318.
61. Motley DC. Physical experimentation and actuated wheel design for granular locomotion using Resistive Force Theory [PhD Thesis]. Massachusetts Institute of Technology; 2016.
62. Yang R, Jayasundara C, Yu A, Curry D. DEM simulation of the flow of grinding media in IsaMill. *Miner Eng*. 2006;19(10):984-994.
63. Taberlet N, Newey M, Richard P, Losert W. On axial segregation in a tumbler: an experimental and numerical study. *J Stat Mech: Theor Exp*. 2006;2006(07):P07013.
64. Stewart R, Bridgwater J, Zhou Y, Yu A. Simulated and measured flow of granules in a bladed mixer–a detailed comparison. *Chem Eng Sci*. 2001;56(19):5457-5471.
65. Alizadeh E, Bertrand F, Chaouki J. Comparison of DEM results and Lagrangian experimental data for the flow and mixing of granules in a rotating drum. *AIChE J*. 2014;60(1):60-75.
66. Lommen S, Schott D, Lodewijks G. DEM speedup: stiffness effects on behavior of bulk material. *Particuology*. 2014;12:107-112.
67. Ucgul M, Fielke JM, Saunders C. Defining the effect of sweep tillage tool cutting edge geometry on tillage forces using 3D discrete element modelling. *Inform Process Agric*. 2015;2(2):130-141.
68. Wong J. Predicting the performances of rigid rover wheels on extraterrestrial surfaces based on test results obtained on earth. *J Terramechan*. 2012;49(1):49-61.

*Manuscript received Jun. 28, 2018, and revision received Nov. 9, 2018.*

# Supplementary Material

**Andrew Thoesen**[1] | **Sierra Ramirez**[1] | **Hamid Marvi**[1]

## SUPPLEMENTARY MATERIAL

### | Mathematical Model of an Archimedes Screw with Cartesian Coordinates

To address the forces of granular media on a uniform Archimedes screw with analytical methods, it first becomes necessary to define the screw in Cartesian space to describe its motion. To be more specific mathematically, we are using a right-handed helicoid. The equation of a helicoid is given by defining the Cartesian coordinates with their parameterized counterparts:

$$x = r\cos(\theta) \quad y = r\sin(\theta)\, z = p\theta \tag{1}$$

This defines the $x$, $y$, $z$ coordinates based on the radius of the helix, the chosen pitch, and the rotation with respect to the $z$-axis. We are then able to define the center locations of discretized plates as shown in figure 11. With the surface curvature defined by the coordinates, as well as location, we can determine the direction of the normals. We obtain the normal vectors for the primary planes by using the respective Jacobian of each component:

$$J_x = \begin{vmatrix} \partial y/\partial r & \partial z/\partial r \\ \partial y/\partial \theta & \partial z/\partial \theta \end{vmatrix} = psin(\theta) \tag{2}$$

$$J_y = \begin{vmatrix} \partial z/\partial r & \partial x/\partial r \\ \partial z/\partial \theta & \partial x/\partial \theta \end{vmatrix} = -pcos(\theta) \tag{3}$$

$$J_z = \begin{vmatrix} \partial x/\partial r & \partial y/\partial r \\ \partial x/\partial \theta & \partial y/\partial \theta \end{vmatrix} = r \tag{4}$$

From the magnitude of the normal vectors in eq(5), the unit normal vectors are then developed. These are the direction cosines for the surface normals. These are the cosines of the angle away from a primary axis. For instance, if $z_n$ = 1, then its angle away from the $z$-axis is 0; it is aligned entirely on the z-axis. The $x_n$ and $y_n$ would then be 0, and their respective angles 90° because the normal vector is perpendicular to both directions.

$$L = \sqrt{psin(\theta)^2 + pcos(\theta)^2 + r^2} = \sqrt{p^2 + r^2} \tag{5}$$

$$x_n = \frac{psin(\theta)}{\sqrt{p^2 + r^2}} \quad y_n = \frac{-pcos(\theta)}{\sqrt{p^2 + r^2}} \quad z_n = \frac{r}{\sqrt{p^2 + r^2}} \tag{6}$$

In figure 11, the normal vectors of a target helix have been generated and laid over a CAD model for verification.

## | Applying the RFT Model

The equations for resistive force theory [1] are simplified below. $\beta$ and $\gamma$ are the angle of a horizontal plate away from the horizontal plane, and the angle of attack of velocity from the horizontal plane, respectively. These angles are evaluated from a perspective defined by assuming a horizontal screw pushing material sideways. While the screw rotates, the material sees a sideways movement in small, discrete timesteps. In this fashion, $\gamma = 0$ consistently. $\beta$ of each plate varies depending on the position around the screw radially. $z_n$, therefore, determines how our approximated plates are tilted towards the main axis of the screw. This happens in a radial fashion around the screw axis and our evaluation relies on a key assumption from later work [2] in testing granular intruders: that horizontal tilting of an intruder's orientation results in similar forces to vertical tilting of an intruder's orientation. If there is sideways motion, then $\beta$ applied to pitch or yaw produces roughly similar forces in that axial direction.

The model used for this interpretation is given in figure 10. We chose to lift the two-dimensional model from the literature and apply it as an approximation to our three-dimensional screw. We used this interpretation to try to estimate thrust force; if we change the plane our ability to predict thrust disappears. The change in a point translating along a helix's curve is related by the equations of its pitch and radius. The translational and rotational motion are coupled. If this screw were not static, it would travel forward in a horizontal path (with slight offset due to handedness). For a static screw, during a discrete timestep, while the actual contact point on the screw rotates in a circle around the axis, small, discrete, horizontal strips of the granular media appear to be pushed forward by a discrete plate element. What an individua grain sees is a small, continuous push in the horizontal direction as the helical surface rolls over it while appearing to translate sideways. This is the interpretation we evaluated because we could not evaluate thrust with this approach otherwise. The coefficients are those utilized for 3 mm glass beads in the literature [1], as they appeared to be of acceptable similarity.

Two $\alpha$ parameters, which are the depth-independent, pressure factors for each section in both an axial and outward direction are functions of these angles. Since $\gamma = 0$, the equations from the resistive force theory [1] for $\alpha$ simplify to those below

$$\alpha_{i,Outward} = A_{00} + A_{10}\cos(2\beta) + B_{11}\sin(2\beta) + B_{-11}\sin(-2\beta) \tag{7}$$

$$\alpha_{i,Thrust} = C_{11}\cos(2\beta) + C_{01} + D_{11}\sin(2\beta) \tag{8}$$

These $\alpha$ are then multiplied by the respective surface areas for each plate, leading to the depth-independent force. The results are multiplied by their respective depth with matrices and summed:

$$F_{Thrust} = \sum \overline{\alpha}_{i,\,Thrust} * \overline{A}_i$$

$$F_{Outwards} = \sum \overline{\alpha}_{i,\,Outwards} * \overline{A}_i$$

We also explored how discretizing plates may affect the results. The MATLAB code was tested at discretized plate dimensions of 1-5 mm sides with no difference observed in the estimated forces.

## REFERENCES

[1] Li C, Zhang T, Goldman DI. A terradynamics of legged locomotion on granular media. science 2013;339(6126):1408–1412.

[2] Askari H, Kamrin K. Intrusion rheology in grains and other flowable materials. Nature materials 2016;15(12):1274.